JOURNAL OF COMPUTATIONAL PHYSICS 12, 234–246 (1973)

# Calculating Three-Dimensional Free Surface Flows in the Vicinity of Submerged and Exposed Structures*

B. D. NICHOLS AND C. W. HIRT†

*University of California, Los Alamos Scientific Laboratory, Los Alamos, New Mexico 87544*

Received May 19, 1972

A numerical technique has been developed for calculating the three-dimensional, transient dynamics of incompressible fluid having a free surface. The Navier–Stokes equations are solved by a solution algorithm based on the Marker-and-Cell method. The flow may be calculated around variously shaped and spaced obstacles that are fully submerged or penetrate the surface. To illustrate the capability of this technique a variety of examples are presented.

## INTRODUCTION

The recent development of a general method for the numerical calculation of three-dimensional, incompressible, transient fluid flow [1] has provided a means of studying many effects heretofore not calculable by numerical methods. As initially developed this method solves the Navier–Stokes equations for an incompressible, confined flow over and around variously shaped and spaced obstacles, and is based on a variant of the original Marker-and-Cell method [2] for two-dimensional flow. In this paper an extension of the new three-dimensional technique is presented that permits the calculation of free surface flows in the vicinity of submerged and exposed obstacles. A number of sample calculations are included to demonstrate the wide application of this new capability.

## THE NUMERICAL METHOD

The Marker-and-Cell method is a finite-difference technique for calculating the time dependent motion of a viscous, incompressible fluid having a free surface. A stationary network of rectangular cells is utilized to divide the calculational

* This work was performed under the auspices of the United States Atomic Energy Commission and was partially supported by the Office of Naval Research, Government Order NAonr-13-72.

† Now with Science Applications, Incorporated, 1250 Prospect Plaza, La Jolla, California 92037.

region into a finite number of elements with which the fluid variables are associated. The dimensions of a three-dimensional cell are given by $\delta x$, $\delta y$, and $\delta z$. The fluid behavior is computed using finite-difference approximations to the Navier–Stokes equations and equation of continuity. The components of velocity $(u, v, w)$ are specified at the cell faces to which they are normal. For example, the $x$-component of velocity, $u_{i+\frac{1}{2},j,k}$, is located at the center of the boundary between cell $(i, j, k)$ and cell $(i + 1, j, k)$, where the indices refer to cells counted out from the mesh origin. Fluid pressures, $p_{i,j,k}$, are specified at the center of each cell containing fluid, and the free surface is defined by its height, $h_{i,j}$, above the $z = 0$ plane, in the center of each cell column $(i, j)$. For simplicity the surface is assumed single valued with respect to $z$.

A numerical solution for the fluid flow is achieved by advancing the fluid configuration through a series of small time increments $\delta t$. Mass and momentum conservation are assured through the use of conservative finite-difference equations. The solution to the momentum equations is obtained in two steps. Initially an explicit calculation is performed that uses the previous-time velocities and pressures to determine accelerations. Fluid incompressibility is not necessarily assured in this part of the calculation; therefore, the initial velocity field must be adjusted. An iterative algorithm is used for this purpose that adjusts the velocities through changes in the pressure field. This final step was accomplished in the original Marker-and-Cell method by solving a Poisson equation derived from the condition that the velocity divergence at the end of the time step be zero.

The solution algorithm used in the technique reported here is somewhat different in detail, but not in spirit. The basic solution technique has been previously reported in detail [1, 3, 4], but the essence of the algorithm is as follows. The pressure in each Eulerian cell is adjusted proportional to the negative of the velocity divergence $D = \nabla \cdot \mathbf{u}$. The idea behind this can be understood intuitively by noting that if $D$ in a cell is positive the fluid pressure must decrease to reduce $D$, while a negative $D$, corresponding to a net mass inflow, requires an increase in cell pressure.

A pressure leading to a zero divergence can be obtained by simultaneously iterating the pressure and velocity fields, first calculating a pressure change caused by a nonzero $D$, then adjusting the velocities to get a new $D$, etc. Thus, for cell $(i, j, k)$, the pressure changes according to

$$p_{i,j,k}^{l+1} = p_{i,j,k}^{l} + \delta p_{i,j,k}, \tag{1}$$

where $l$ is the iteration number,

$$\delta p_{i,j,k} = -\beta D_{i,j,k} \tag{2}$$

and

$$\beta = \frac{1}{2\delta t((1/\delta x^2) + (1/\delta y^2) + (1/\delta z^2))}. \tag{3}$$

Then each velocity component specified on a face of cell $(i, j, k)$ is adjusted according to the pressure change; for example

$$u^{l+1}_{i+1/2,j,k} = u^{l}_{i+1/2,j,k} + (\delta t/\delta x)\, \delta p_{i,j,k}$$
$$u^{l+1}_{i-1/2,j,k} = u^{l}_{i-1/2,j,k} - (\delta t/\delta x)\, \delta p_{i,j,k}\,. \tag{4}$$

If the cell being considered is a surface cell, that is, one in which the fluid surface is located, the pressure is calculated by a linear interpolation or extrapolation from the pressure in the fluid cell immediately below. Thus,

$$p_{i,j,k} = \eta p_a + (1 - \eta)\, p_{i,j,k-1}\,, \tag{5}$$

where $p_a$ is a pressure applied at the free surface, $\eta = \delta z/d$, and $d$ is the distance from the surface to the center of the cell below. If the cell below the surface cell is an obstacle or rigid boundary cell, indicating the local fluid depth is less than $\delta z$, then a hydrostatic pressure is calculated and set in the cell. In either of these cases $\delta p_{i,j,k}$ must also be determined for the velocity calculations.

## Free Surface Conditions

The fluid surface is single-valued and is initially defined by specifying the surface height above the bottom of the mesh. The surface height is defined at the center of each vertical column of cells in the three-dimensional mesh. This idea was first employed in a MAC-like program by Chan [5] for two-dimensional free surface flows.

The change in the surface elevation is determined by the local fluid velocity, that is, by the vertical component of the fluid motion plus the horizontal convection of the surface elevation from adjacent cell columns,

$$(\partial h/\partial t) = w - u(\partial h/\partial x) - v(\partial h/\partial y). \tag{6}$$

The finite-difference approximation of this equation is written using a space-centered, forward-in-time differencing method. This particular difference approximation is unstable because of a negative diffusion truncation error, see [6], but this error can be compensated for by adding to the surface height equation a positive diffusion term

$$\gamma((\partial^2 h/\partial x^2) + (\partial^2 h/\partial y^2)), \tag{7}$$

where $\gamma$ is a constant diffusion coefficient, chosen greater than $(\delta t/2)$ max $(u^2, v^2)$ to insure stability. Other difference approximations could be used [5] that do not require the explicit addition of stabilizing terms, but as shown in Ref. [6] these

forms are basically the same as that used here. The complete finite-difference form of the kinematic surface equation is, therefore,

$$h_{i,j}^{n+1} = h_{i,j}^{n} + \delta t \left\{ \bar{w}_{i,j,k}^{n+1} + \frac{1}{4\delta x}(u_{i+1/2,j,k}^{n+1} + u_{i-1/2,j,k}^{n+1})(h_{i-1,j}^{n} - h_{i+1,j}^{n}) + \frac{1}{4\delta y}(v_{i,j+1/2,k}^{n+1} + v_{i,j-1/2,k}^{n+1})(h_{i,j-1}^{n} - h_{i,j+1}^{n}) + \gamma \left[ \frac{1}{\delta x^2}(h_{i+1,j}^{n} - 2h_{i,j}^{n} + h_{i-1,j}^{n}) + \frac{1}{\delta y^2}(h_{i,j+1}^{n} - 2h_{i,j}^{n} + h_{i,j-1}^{n}) \right] \right\}, \quad (8)$$

where the indices $i, j, k$ refer to the cell in which the surface is located, $n$ denotes the calculation time cycle, and $\bar{w}_{i,j,k}$ is the vertical velocity at the surface, obtained by linear interpolation between the $w$-velocity at the top and bottom faces of the surface cell.

The free surface boundary conditions require a determination of the normal and tangential velocities immediately outside the surface. These velocities are chosen to satisfy the appropriate free surface stress conditions. However, the complete viscous stress conditions as described in [7] have not yet been incorporated. In this paper only the conditions appropriate for an inviscid fluid will be discussed.

As in the original Marker-and-Cell method, velocities normal to the surface are set to satisfy the incompressibility condition in surface cells. The tangential velocities $(u, v)$ in the cells immediately outside the fluid are obtained by setting them equal to the adjacent interior values, which is consistent with zero shear stress at the surface.

## Wall Boundary Conditions

The calculational mesh is surrounded by a one-cell-thick layer of cells, which are used for setting boundary conditions. The boundaries may be free-slip or no-slip walls, or any part of a boundary may be an inflow or outflow boundary. In addition, any interior cell may be designated as an obstacle cell, in which case it contains no fluid and its edges are treated as rigid boundaries. These obstacle cells may be located anywhere within the mesh and anywhere relative to the free fluid surface, that is, they may be completely submerged, or they may extend through the fluid surface. Any configuration of obstacle cells may be specified, and in this way a great deal of flexibility is achieved in obstacle shapes.

The condition applied to rigid no-slip wall boundaries requires zero tangential velocity at each boundary, while for free-slip boundaries the shear-stress is zero. In both cases the velocity normal to the wall is zero. A prescribed inflow simply requires the setting of the chosen velocity at the boundary cells.

The continuative boundary condition is the most difficult to set properly. The scheme found to have little upstream effect is to require a zero gradient of the tentative velocities (obtained before the pressure iteration) normal to the boundary. These velocities are set at the beginning of each time cycle and are then adjusted during the pressure iteration in the same manner as interior cell velocities. Since $\delta p$ is calculated in surface cells, this same condition is applied for surface cells adjacent to a continuative boundary. A zero shear stress condition is also used at a continuative boundary.

## Numerical Stability Conditions

The conditions necessary to prevent numerical instabilities in the three-dimensional finite-difference approximations are only slightly changed from their two-dimensional counterparts. The distance the fluid travels in one time increment must be less than one space increment. This restricts the time increment to

$$\delta t < \min\left(\frac{\delta x}{|u|}, \frac{\delta y}{|v|}, \frac{\delta z}{|w|}\right). \tag{9}$$

When the viscous diffusion terms are important the condition necessary to insure stability through successive time steps is

$$\nu\delta t < \frac{1}{2}\left(\frac{\delta x^2\,\delta y^2\,\delta z^2}{\delta y^2\,\delta z^2 + \delta x^2\,\delta z^2 + \delta x^2\,\delta y^2}\right), \tag{10}$$

in which $\nu$ is the kinematic viscosity coefficient. The free surface capability adds an additional stability condition. It is necessary to insure that the distance a surface wave travels during one time increment be less than the horizontal cell dimension. This condition can be approximately written as

$$c\delta t < \min(\delta x, \delta y), \tag{11}$$

where $c$ is the wave speed.

There are two additional kinds of instability related to the occurrence of truncation errors that have the form of "negative" diffusion. These conditions, which are fully described in [1] and [6], generally require choosing a value of viscosity large enough to satisfy the condition

$$\nu > \max\left[\left(\frac{\delta t}{2}u^2 + \frac{\delta x^2}{2}\frac{\partial u}{\partial x}\right), \left(\frac{\delta t}{2}v^2 + \frac{\delta y^2}{2}\frac{\partial v}{\partial y}\right), \left(\frac{\delta t}{2}w^2 + \frac{\delta z^2}{2}\frac{\partial w}{\partial z}\right)\right]. \tag{12}$$

The use of viscosity satisfying (12) does not necessarily impose an excessively stringent restriction on the magnitude of Reynolds number that can be calculated,

especially if the truncation error analysis is utilized to derive a local correction to remove the destabilizing effects. Alternatively, we could use other finite-difference approximations, such as the donor cell instead of the space-centered differencing method employed here. The resulting truncation errors, however, may then be excessively diffusive [6], leading to severely inaccurate Reynolds number interpretations. In any case, truncation errors exist and must be considered for any finite-difference scheme. If the nature of the calculation requires a precisely specified viscosity, it is possible to add this in after removal of the truncation errors to the desired order of $\delta t$ and $\delta x$. However, if the flow variations to be calculated can really be adequately resolved by the mesh, then such stabilizing viscous stresses, as proposed previously, are generally negligible. This point is more fully discussed in Ref. [7, 8].

It was reported by Chan and Street [5] that the Marker-and-Cell method was stable when run with $\nu = 0$, and with their improved free surface treatment. It is now believed that this conclusion holds only for certain special cases, especially those in which the regions of negative truncation diffusion translate relative to the Eulerian mesh. Indeed, their same problem (propagation of a solitary wave down a wave tank) has been run with the method reported here, and with $\nu = 0$. No visible instabilities were created. In this particular case, one of the truncation error terms that can contribute a negative viscosity arises from the horizontal velocity gradient. On the leading edge of the solitary wave this makes a positive contribution to the effective viscosity. On the trailing edge of the wave this term makes a negative contribution that could lead to an instability. The wave speed in these calculations was such that a local disturbance would be amplified for only approximately 25 time steps. Consequently, any short wavelength disturbance existing in this region would not have time to grow to an observable magnitude.

## Data Display

Presentation of data from a three-dimensional calculation in an easily comprehensible form is difficult. An effective technique is to display such data as velocity fields, surface configurations, etc., using computer generated perspective pictures. For this purpose a hidden-line perspective view plot routine, developed especially for displaying data in an Eulerian mesh, has been recently developed [9]. Three-dimensional stereoscopic views of data plots can be made by constructing two perspective pictures from slightly separated viewing points and viewing them in a stereo-slide viewer.

To observe velocity fields, velocity vectors may be plotted for any chosen combination of cells in the mesh. Velocities plotted in selected planes in a region of interest can give a fairly good idea of the flow, but sometimes it is still difficult

to visualize the full three-dimensional flow pattern. This can often be remedied by plotting in stereo all the velocity vectors in a selected volume of interest. Sometimes only portions of a flow field are plotted, thus emphasizing special regions of interest. This has been used effectively, for example, to observe the structure of an eddy formed in the wake of an obstacle.

Surface configurations can be plotted in perspective by first computing the elevation of the surface at each vertical mesh line. These elevations are obtained by averaging the surface heights, $h_{i,j}$, in the four adjacent cell columns. The surface is then constructed by connecting lines between pairs of elevation points. The $h_{i,j}$ points themselves could be connected in this way, but undesirable gaps would be left near all mesh boundary and obstacle walls.

The transient contortions of a surface are most effectively displayed by making motion pictures of the surface in perspective. In most instances, the time step used for an optimum numerical solution is also a reasonable time step for the interval between movie frames.

## Calculational Examples

To demonstrate the capability of this three-dimensional free surface technique, a variety of examples have been run on a CDC 7600 computer. All of the problems shown here used only the 64,000 word fast core memory. A large core memory is also available, which makes an additional 400,000 words accessible. Since the large core memory is not a direct access core, its use does slow down the calculational speed somewhat. Typical calculation times vary from 2.64 seconds per time cycle for a problem with 3360 calculational cells, to 10.34 seconds per time cycle for flow in a mesh of 6336 cells. In the latter case (not illustrated in this paper) the large core memory was used.

Test problems include some nearly-inviscid two-dimensional problems run to compare with previous numerical calculations and analytical studies, and some three-dimensional problems of fluid flowing over and around obstacles, which have not previously been calculable.

An example of a two-dimensional test calculation involves the generation of waves in a tank by a piston at one end of the tank. A typical calculation consists of a mesh of $68 \times 2 \times 10$ interior cells in the $x$, $y$, $z$-directions, respectively. To actuate a piston by moving it at one end of the mesh creates a problem, since all mesh boundaries are stationary. This difficulty was overcome by applying an acceleration to the fluid instead, that is, by adding to the initial $u$-equation each cycle an acceleration equal to

$$\ddot{x}_p = -A\omega^2 \cos \omega t, \tag{13}$$

where $A$ represents the piston amplitude and $\omega$ the piston frequency. The point of view taken here is that the mesh is attached to the piston and is, therefore, moving with respect to the laboratory frame of reference. The mesh boundaries have rigid, free-slip conditions applied on all except the right-hand boundaries, which is a continuative boundary that allows fluid to flow in or out. This simulates the motion of a piston at one end of the tank without the generation of waves at the other, continuative, end.

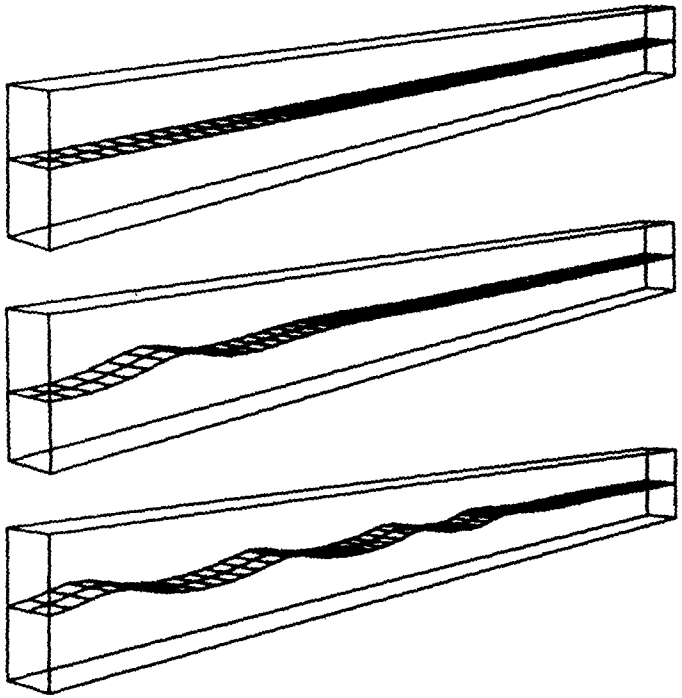

FIG. 1. Perspective view of the surface configuration generated by a periodic piston at times 0., 10., and 24.

Shown in Fig. 1 are perspective view plots of the fluid surface. In nondimensional units the initial fluid height is 1.02, the piston amplitude is 0.10, and the mesh has square cells with edge length 0.20. The period of the piston is 5.22. Therefore, from the relation [10],

$$\omega^2 = gk \tanh kd, \tag{14}$$

where $g = -1.0$ is the gravitational acceleration and $k$ is the wave number, the expected wavelength is 4.00, and the calculated wave speed is 0.77. The measured wavelength is $4.05 \pm 0.10$ and the measured wave speed is $0.80 \pm 0.03$, showing good agreement with the theoretical results.

An analytical solution has been given for the surface elevation in this problem [11]. The numerical surface elevation at early times compares very well with the analytical results, although some amplitude damping from viscous dissipation is observed as the waves progress down the tank.

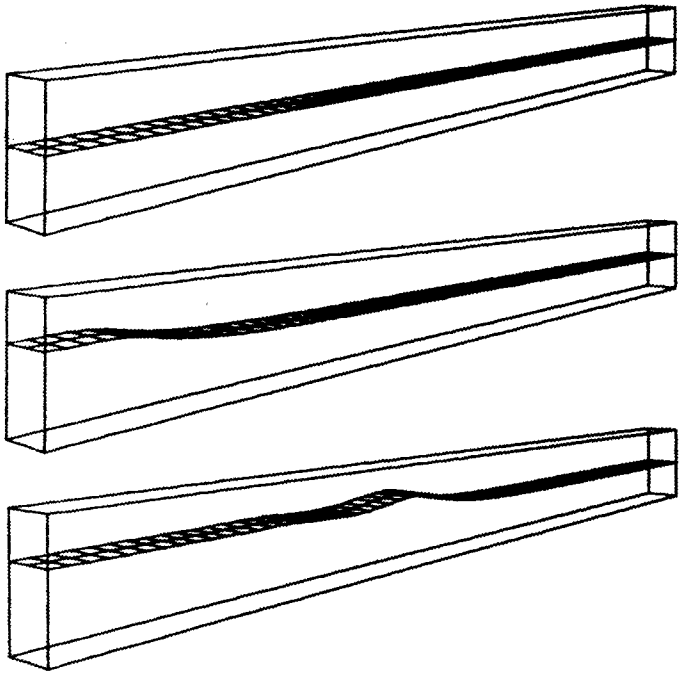

FIG. 2. Perspective views of the surface of an undular bore at times 0., 5., and 15.

A bore can be generated by uniformly accelerating the piston, as described before, over some time interval $t_0$, as seen in Fig. 2. By choosing the piston Froude number, which is based on the initial fluid depth and final piston velocity, such that the change in fluid depth is much less than the initial depth, a nonbreaking, undular bore is formed.

Several undular bore calculations were done with a piston Froude number of 0.2475. The initial depth of the fluid was vertically resolved in six cells, while 68 cells were used in the downstream direction. Piston accelerations were applied during one time step for both $t_0$ of 0.01 and 0.10, while for $t_0$ of 1.00 the acceleration was applied over ten time steps. The calculated late time elevation change in units of the initial elevation for all of these runs was 0.2627 with a persistent slight oscillation in time of $\pm 0.0001$. This is to be compared with a long wave theory prediction of 0.2628 [12]. For a $t_0$ of 3.00, applied over 30 time steps, the elevation change was

the same, but the slight oscillations were gone. When the acceleration was applied more slowly, over 100 time steps for a $t_0$ of 10.00, the calculated elevation change agreed with the theoretical value of 0.2628.

The three-dimensional capability of this technique is demonstrated with three examples of flow around obstacles. In all cases the obstacles are contained in a $15 \times 15 \times 7$ cell mesh. The boundary at $x = 0$ is an input boundary, and the opposite end of the mesh is an outflow boundary with continuative boundary conditions. All other boundaries are free-slip rigid walls.

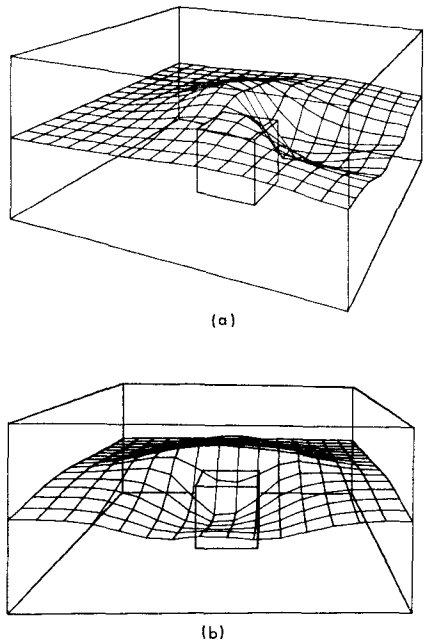


FIG. 3. Perspective views of the surface configuration resulting from flow over a submerged obstacle as seen from the side (a) and downstream (b).

The flow over a submerged obstacle is shown in Fig. 3. The $3 \times 3 \times 3$ cell obstacle is immersed in a fluid initially 3.5 cells deep. The flow Froude number is 2.0, based on initial fluid depth and input velocity. Plots are shown in Fig. 3 at a time of 2.0, after 20 calculational time cycles. Views from two separate viewing positions are shown: plot (a) shows the fluid flowing through the mesh from left to right; plot (b) is viewing the flow from a centered, downstream position. The advantages of having a "transparent" surface plot are demonstrated here. Not only is the obstacle visible through the surface, but none of the surface itself is hidden from view.

As previously mentioned, the surface configuration is best viewed in stereo, but this is difficult for many people without a special viewing instrument. Nevertheless, it can be done with a little practice. Figure 4 shows the views for both eyes, viewing the submerged obstacle from the side. This view will appear in stereo by holding the pair of pictures at a comfortable viewing distance, slightly crossing the eyes, and focusing in front of the picture [9]. The persistent viewer should be able to bring these views into a single stereo image lying somewhere between the eyes and the pictures.

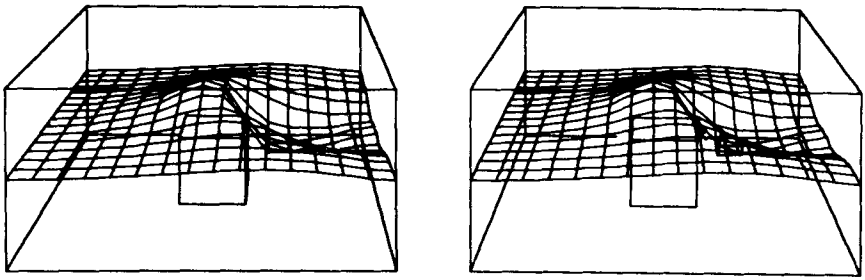

FIG. 4. The two perspective views appear as a single stereo picture when viewed with eyes "slightly crossed."

A calculation of flow in the vicinity of a vertical structure such as a pile is shown in Fig. 5. Fluid is flowing around a $3 \times 3 \times 7$ cell obstacle with flow Froude number 1.06. The gap between the surface and the front of the obstacle is inherent in our present perspective view plot routine. Gaps such as these, which are less than a cell width, are permitted in payment for a large increase in plotting speed [9].

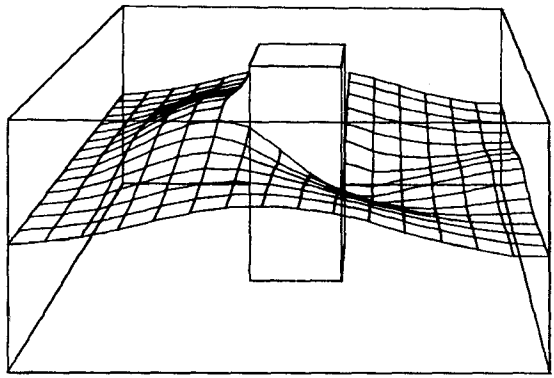

FIG. 5. Perspective view of the surface configuration resulting from flow past a rectangular pile.

Figure 6 shows a similar study: flow past a $2 \times 5 \times 7$ cell obstacle, with a Froude number of 0.82. As expected, an eddy tries to form behind the obstacle; however, it comes and goes at regular intervals. This behavior is coupled with a rise and fall of the fluid elevation behind the obstacle; the eddy forms as the depth behind the obstacle increases and disappears as it falls. The period of the undulations is not affected by increasing the length of the mesh by an additional five cells. The initial conditions for this calculation employ a uniform $u$ velocity, equal to the continuous input velocity, with $v$ and $w$ velocities zero.

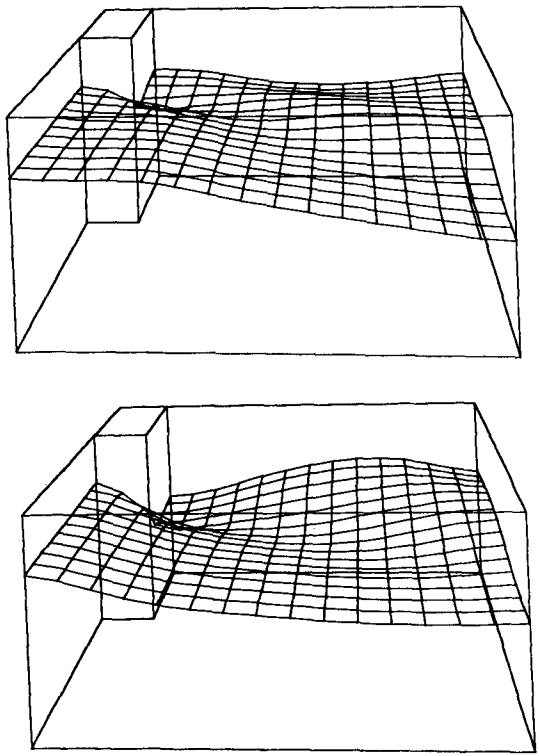

FIG. 6. Perspective views of the surface configuration resulting from flow around a wide obstacle at slightly different times.

Another initial condition is obtained by placing a "frictionless lid" on the surface (accomplished by placing a horizontal obstacle, with free-slip boundaries, in the plane of cells just above the fluid). This two-dimensional confined flow problem is then run until the flow behind the obstacle is well established; then the "lid" is removed and the normal three-dimensional free surface calculation started. With

these initial conditions the magnitude of the undulations is decreased but their period remains unchanged.

## ACKNOWLEDGMENTS

The authors wish to express appreciation to their colleagues in T-3 for many valuable suggestions, especially J. L. Cook for writing the initial three-dimensional program, and to James Witting, Department of the Navy, Office of Naval Research, for suggesting and encouraging the undular bore calculations.

## REFERENCES

1. C. W. HIRT AND J. L. COOK, *J. Comput. Phys.* **10** (1972), 324.
2. F. H. HARLOW AND J. E. WELCH, *Phys. Fluids* **8** (1965), 2182; J. E. WELCH, F. H. HARLOW, J. P. SHANNON, AND B. J. DALY, Los Alamos Scientific Laboratory Report, LA-3425 (1966).
3. A. J. CHORIN, AEC Research and Development Report, NYO-1480-61 (1966).
4. J. A. VIECELLI, *J. Comput. Phys.* **8** (1971), 119.
5. R. K.-C. CHAN AND R. L. STREET, *J. Comput. Phys.* **6** (1970), 68; R. K.-C. CHAN, R. L. STREET, AND J. E. FROMM, Proc. Second Internat. Conf. Num. Meth. Fluid Dynamics, Berkeley, p. 429 (1970).
6. C. W. HIRT, *J. Comput. Phys.* **2** (1968), 339.
7. B. D. NICHOLS AND C. W. HIRT, *J. Comput. Phys.* **8** (1971), 434.
8. J. A. YOUNG AND C. W. HIRT, *J. Fluid Mech.*, to appear.
9. C. W. HIRT AND J. L. COOK, submitted for publication.
10. J. J. STOKER, "Water Waves," Interscience, New York, 1957.
11. T. H. HAVELOCK, *Phil. Mag.* **8** (1929), 569.
12. J. WITTING, *CRC Critical Reviews in Solid State Sciences* **2** (1972), 555.